Automation and Optimization of Stopping and Range of Ions in Matter Simulation Runtime

Varun S. Vaidyanathan[1,2], David Scrymgeour[1], Michael Titze[1,*]

1: Sandia National Laboratories, Albuquerque, NM, 87123

2: Elmore Family School of Electrical and Computer Engineering, Purdue University, West Lafayette, IN, 47907

*: mictitz@sandia.gov

Abstract

Prior to every ion implantation experiment a simulation of the ion range and other relevant parameters is performed using Monte-Carlo based codes. Although increasing computing power has improved the speed of these calculations, the demands on Monte-Carlo codes are also increasing, requiring evaluation of the optimal number of simulations while ensuring accuracy within threshold bounds. We evaluate the "Stopping and Range of Ions in Matter" (SRIM) code due to its widespread usage. We show how dividing simulations into multiple parallel simulations with different random seeds can lead to calculation speedup and find lower bounds for the required number of ion traces simulated based on an exemplar system of a Ga focused ion beam and a high energy C beam as used in high linear energy transfer testing. Our results indicate simulations can yield results within the underlying data accuracy of SRIM at 10X and 100X shorter simulation time than the SRIM default values.

Introduction

For decades, ion implantation has been a critical tool for the semiconductor industry[1]. With the advent of focused ion beam (FIB) tools, nanoscale control over material properties is possible[2, 3]. In more recent work, especially involving quantum applications, ion implantation is used for adding functionality by implanting optically active color centers with nanoscale resolution [4-6]. In contrast to ion implantation, where ions are used for functionalizing materials, ion irradiation can be employed for testing the radiation effects on nuclear materials[7] and microelectronics [8]. High-energy ions are used as surrogates for reactor-type neutron or cosmic-ray space environments that are too difficult to replicate in a laboratory setting [9, 10].

Prior to any ion implantation experiment, a simulation of the ion range is required, typically done through a SRIM simulation [11]. Some quantum sensing applications require fabrication of a thick, homogeneously doped, implant layer [12]. For simulation of such implants, many SRIM simulations are required to obtain the individual implant profiles used in fitting to the desired shape [13]. This indicates a requirement for efficiently simulating ion implantation while maintaining high confidence in the simulation result.

Here, we demonstrate that relevant parameters of SRIM simulations, for example ion range, straggle, and vacancy production, can converge to the final accepted result (here taken as the result of 1e5 ion traces), within a < 5 % error with as low as 400 ions. We choose 5 % as the upper error threshold since the SRIM stopping power model is only accurate to no more than 5 % [11]. By using multiple seeds, therefore adding parallelizability of the calculation and averaging over a second dimension, we achieve up to 100 X speedup of the SRIM simulation. We demonstrate the results using a low energy 35 keV Ga beam, as typically found in FIB systems, as well as a 36 MeV C ion, a representative ion used for linear energy transfer testing [14].

Methods

Multiple SRIM simulations were run where parameters were incremented with data collected into a standard file format. Since this process is iterative, we used the PySrim Python library to allow iteration over the relevant parameters [15]. From PySrim, the following objects were used:

- TRIM
- Ion
- Layer
- Target
- Output.Results

Our Pysrim setup and the objects used are shown in Figure 1. This indicates the various options that can be changed in an SRIM simulation with the PySRIM automation:

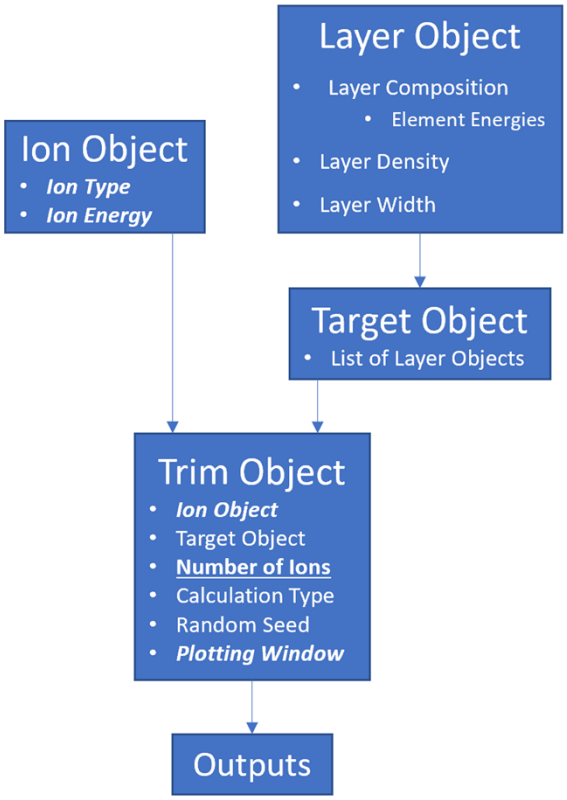

Figure 1: PySrim Workflow. The number of ions parameter (underlined) in the TRIM object was iterated. We also adjust the italic parameters between the high and low energy simulation types.

To generate the data used in the analysis, we adjusted the Number of Ions parameter in the TRIM object and created multiple of these TRIM objects. These TRIM objects are then used by SRIM to generate simulation outputs, and they are automatically run in sequence through the PySrim programming.

In these simulations we explored both low energy and high energy scenarios verify the SRIM operation in different regimes. These scenarios were:

- To represent standard low energy Focused Ion Beam experiments, gallium ions (Ga) with 30 KeV of energy were used.
- To represent standard high energy Linear Energy Transfer experiments, carbon ions (C) with 36 MeV were used.

In both cases, the target material was pure silicon with a density of 2.3212 g/cm^3. The target depth was 800 Å for the low energy Ga experiments and 500000 Å (50 µm) for the high energy C experiments to ensure ions fully range out within the Si layer. The Si layer object used SRIM default parameters, i.e., displacement energy of 15 eV, lattice binding energy of 2 eV, and surface binding energy of 4.7 eV. The target object was made using a list of one element: the Si layer object.

The calculation type within SRIM was set to a Quick-Calculation damage calculation with an output of the ion distributions [13]. The random seed was also deliberately incremented to avoid possible outliers that could occur due to the randomness of the simulations. The plotting window was adjusted between simulation of Ga and C implantation to focus on the areas of the layer where the majority of the ions came to rest. This gives a much higher resolution output within the selected window.

Results

The Asymmetric Gaussian and Lorentzian curves, $\rho(z)$, as a function of depth/range z are represented by the following formulas:

(a) $$\rho_{\mathrm{Gaus}}(z) = \frac{A(1+e^{a(z-z_0)})^2}{4} \exp\left[-\frac{(1+e^{a(z-z_0)})^2}{4}\frac{(z-z_0)^2}{2\sigma^2}\right]$$ (b) $$\rho_{\mathrm{Lor}}(z) = \frac{A\sigma^2}{\sigma^2 + \frac{(1+e^{a(z-z_0)})^2}{4}(z-z_0)^2}$$

Equation 1: Formula for (a) Asymmetric Gaussian curve and (b) Lorentzian curve. In both these formulas, A is the maximum amplitude, a is the asymmetric parameter, z0 is the depth with maximum defect density, and σ is full width at a half maximum.

where the fitting parameters for both equations are a, the asymmetric fitting parameter, A is the amplitude, σ (sigma) is the full width at half maximum, and z0 is the offset in depth, corresponding to the average ion range. The optimize.curve_fit function from the SciPy package was used to automatically fit the generated output data and find the converging value of the fitting parameters that gives a minimized mean-square-error (MSE) [16].

Simulation and Fitting of Varying Numbers of Ions

The low energy Ga and high energy C simulations were simulated using a range of ion numbers to show the effect of ion number on the accuracy of the final simulation for the two different ion beams. Figure 2 and Figure 3 show the averaged results and the best fit curve of the simulations after incrementing the number of ions in a single simulation setup.

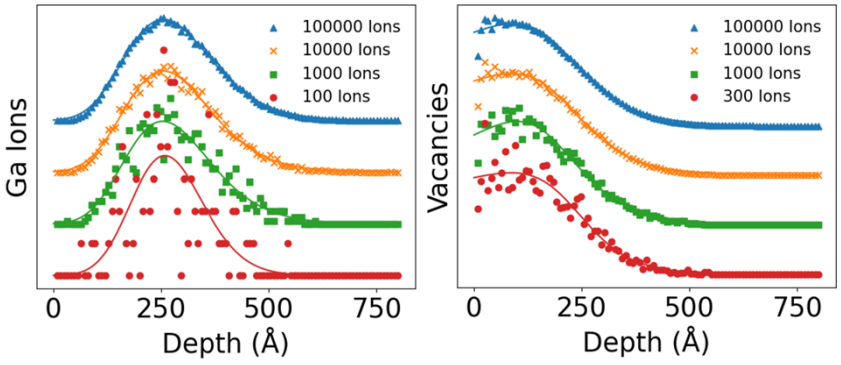

Figure 2: Vertically offset comparisons between increasing number of ions for (a) ion range and (b) ion vacancy for the low energy (30 KeV) Ga beam implanted into Si Layer.

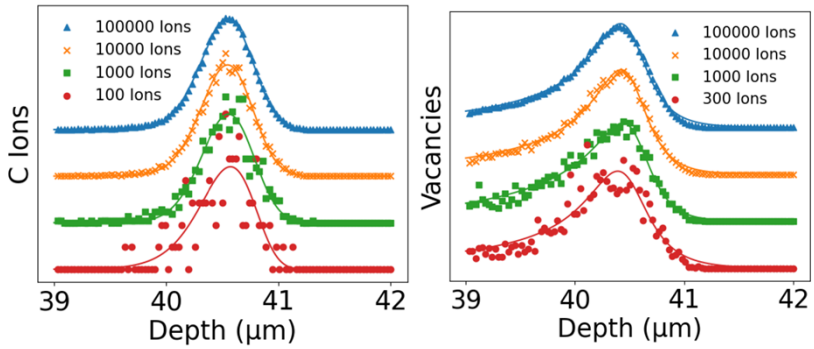

Figure 3: Vertically offset comparisons between increasing number of ions for (a) ion range and (b) ion vacancy for the high energy (36 MeV) C beam implanted into Si Layer.

Figure 2 and Figure 3 show that, as the number of ions increase, the scatter in the curve decreases so that at sufficiently high number of ions, the curves generate a smooth curve that can be fit to the equations in Equation 1 with low MSE. This is true for both the range and vacancy data. For all the simulations we performed, we tracked the total simulation runtime and found the total runtime had a linear relationship to the number of simulated ions. As a result, finding the threshold where increasing the number of ions no longer gives a significant or necessary increase in the curve fitting accuracy allows for an optimal simulation runtime. At this threshold, given that runtime increase is linear, the improved accuracy gained from further increasing the number of ions is not worth the increased runtime cost. By implementing this threshold, simulations can be completed faster, and data can be produced more efficiently, especially for very high energy beam simulations.

Number of Ions Needed to Get the Parameters Within a Threshold Accuracy

We simulated both the low and high energy beams for different seeds to reduce the effects of simulation outliers. Five seed numbers (0-4) were used, and the resulting output averaged for each iteration of the simulation to represent five trials of the same simulation conditions. Both the ion range and vacancy curves converged when increasing the number of ions. We graphed the percent error in these parameters over an increasing number of ions to visualize the convergence in Figures Figure 4 -

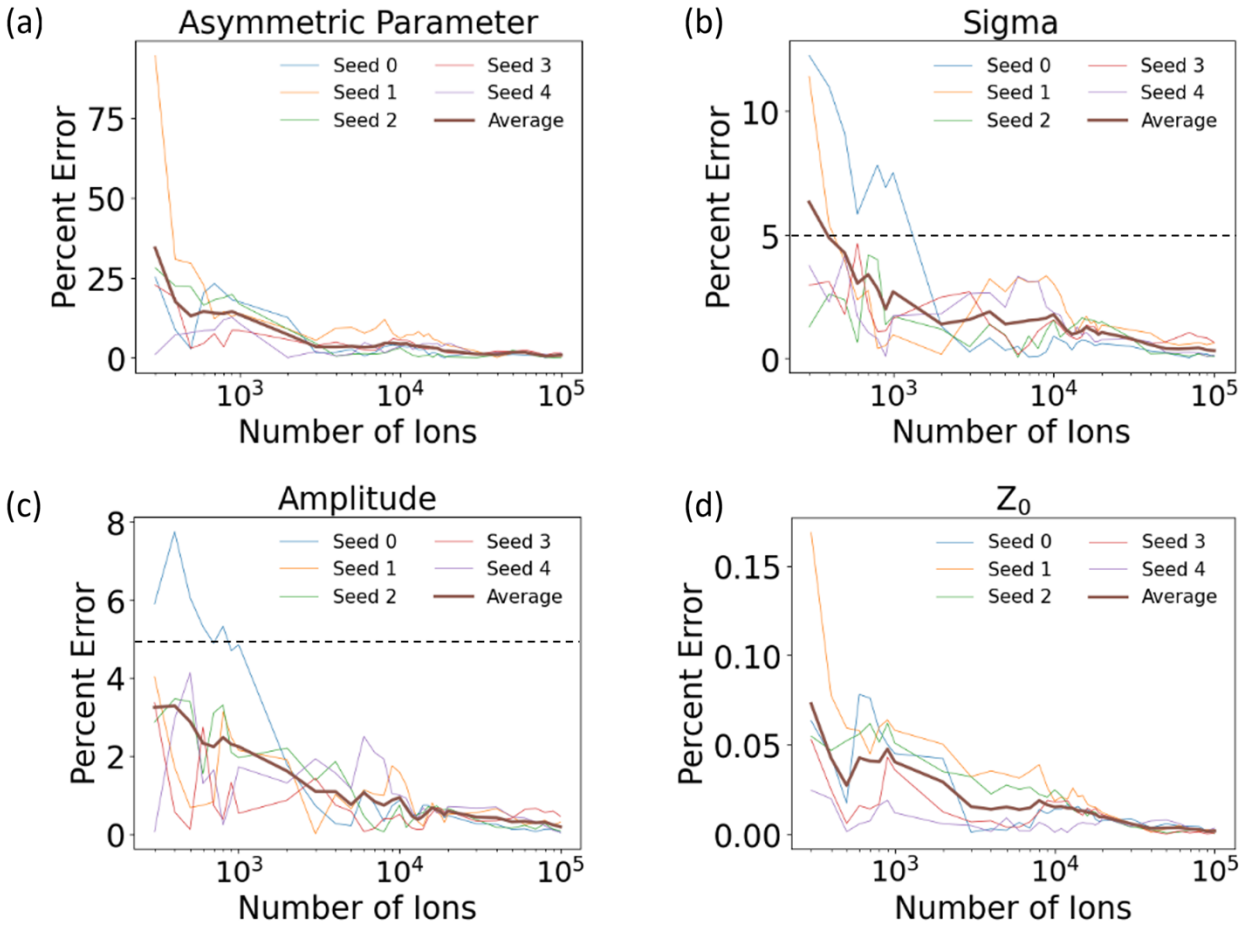

Figure 7. We define the fitted parameter values at 1e5 ions as the correct values, and evaluate the accuracy by comparing the parameters obtained via fitting for varying number of ions simulated against those parameters, as well by averaging over multiple runs using different random seeds.

Shown in Figure 4 &

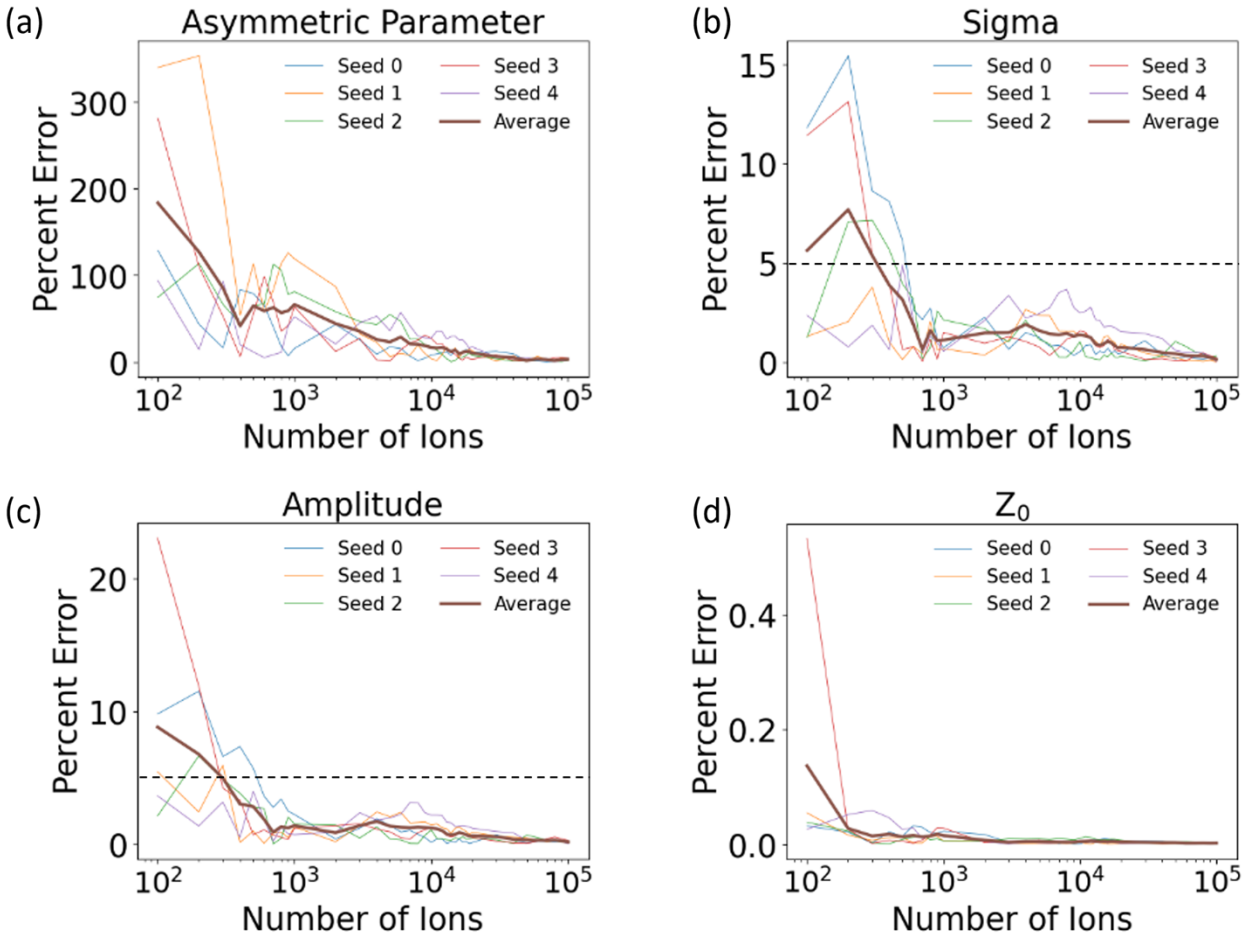

Figure 5 is the decreasing percent error of the simulation as a function of number of ions for the different fitting parameters for Ga (Figure 4) and C (

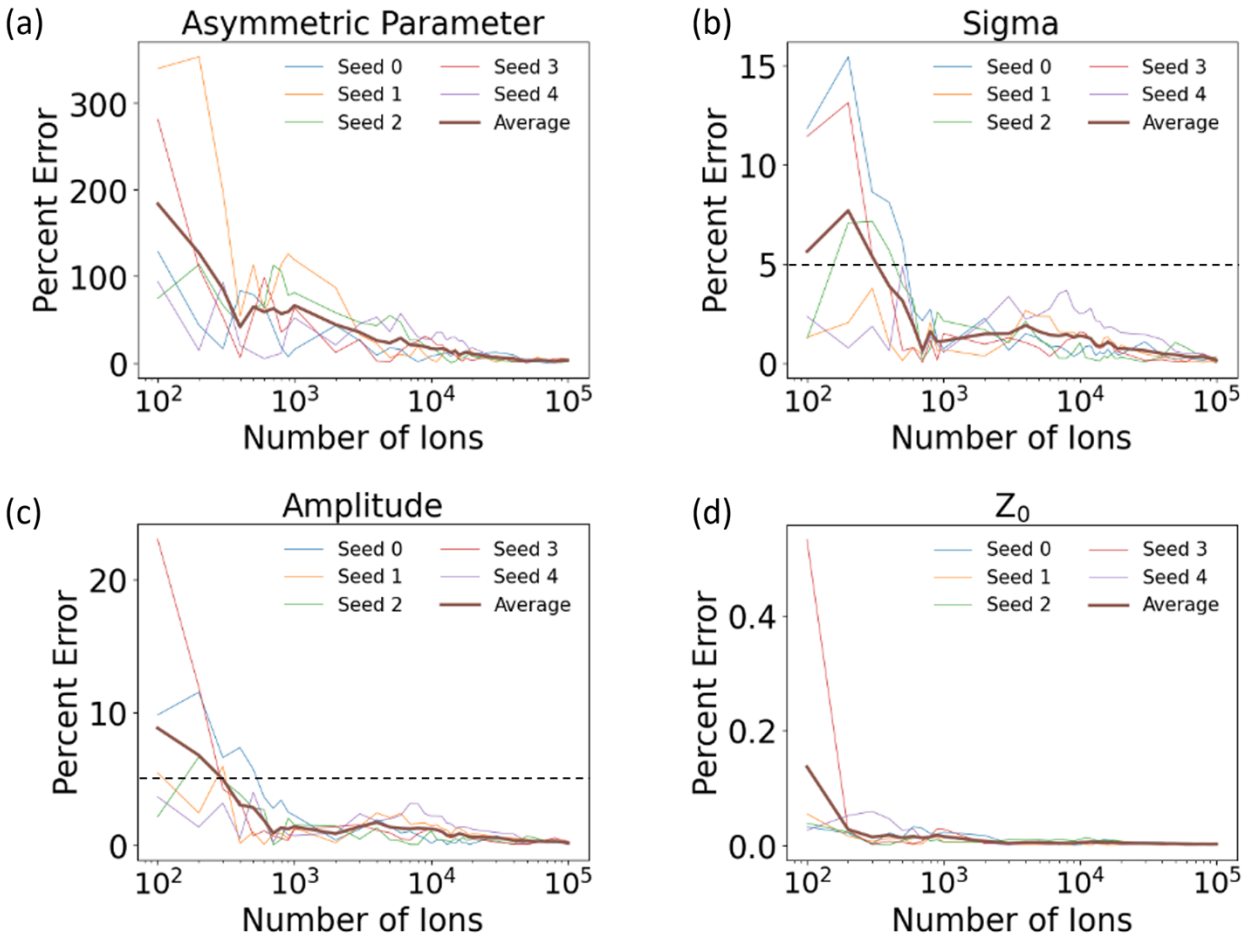

Figure 5). They show convergence of the fitting parameters as the number of ions increases.

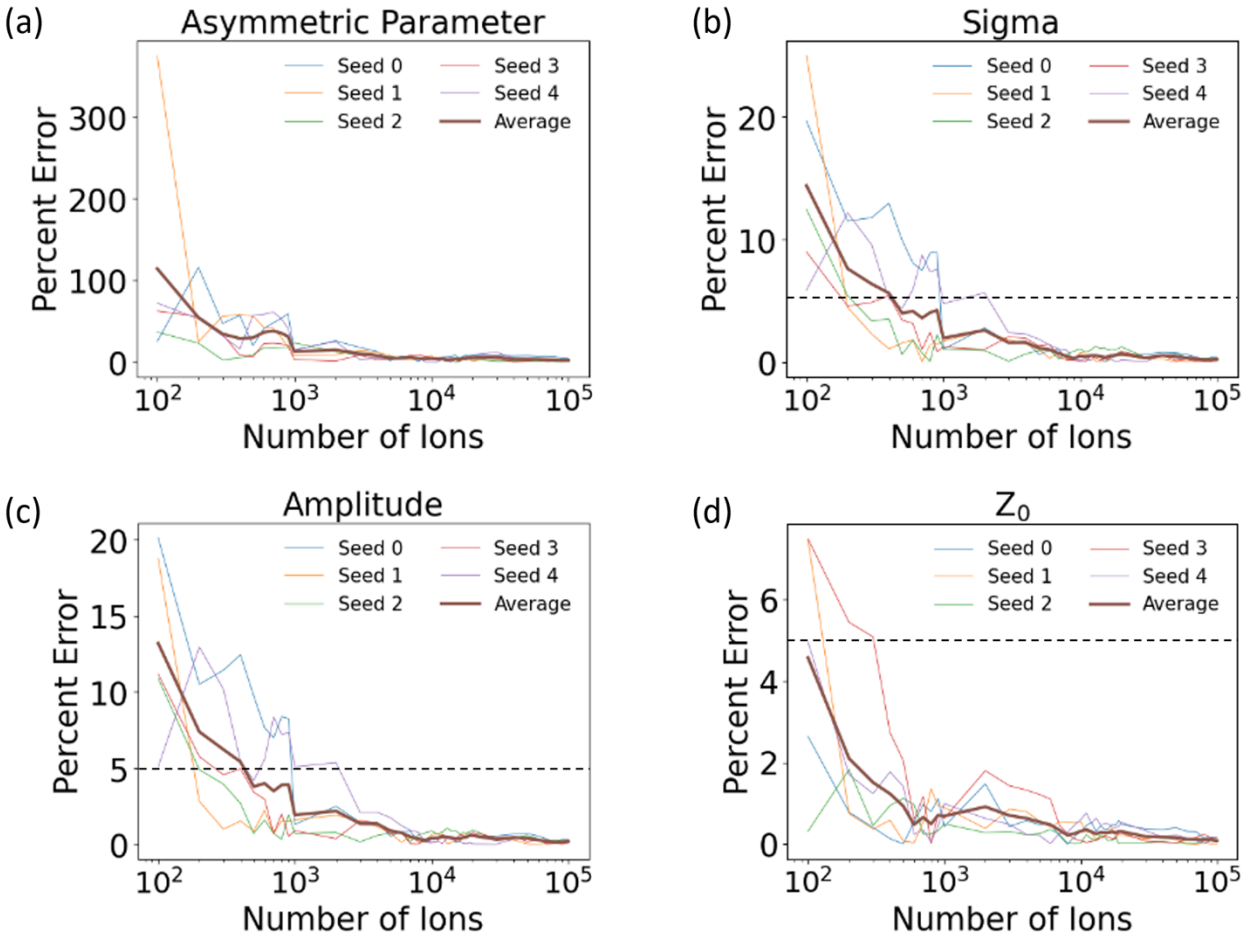

Figure 4: Percent error across an increasing number of ions the 4 fitting parameters of the asymmetric Gaussian curve that was fit to the Ga in Si range data with (a) asymmetric parameter, a (b) sigma, σ full-width half maximum, (c) amplitude, A and (d) ion range, z_0. Five different simulated seed numbers are plotted along with the average of those 5 seed numbers. The average goes towards zero faster than the individual curves indicating a better convergence when averaging multiple seeds compared to using a single seed. The dashed horizontal line denotes the 5 % error threshold.

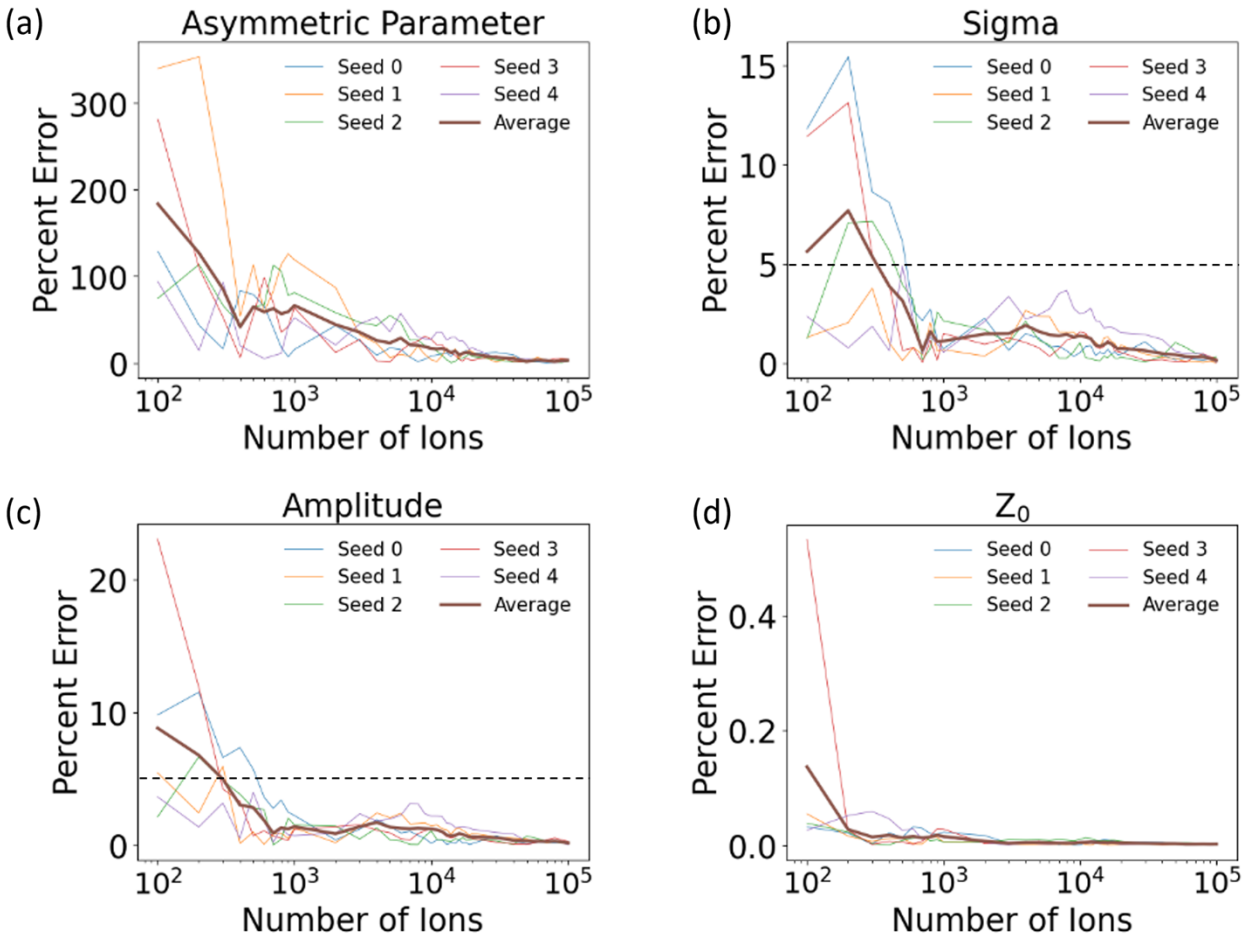

Figure 5: Percent error across an increasing number of ions the 4 fitting parameters of the asymmetric Gaussian curve that was fit to the C in Si range data with (a) asymmetric parameter, (b) sigma, (c) amplitude, and (d) z_0. Five different simulated seed numbers are plotted along with the average of those 5 seed numbers. The average goes towards zero faster than the individual curves indicating a better convergence when averaging multiple seeds compared to using a single seed. The dashed horizontal line denotes the 5 % error threshold. At high energy estimation of the ion range has high relative accuracy, hence all cases have a < 5 % error.

Shown in

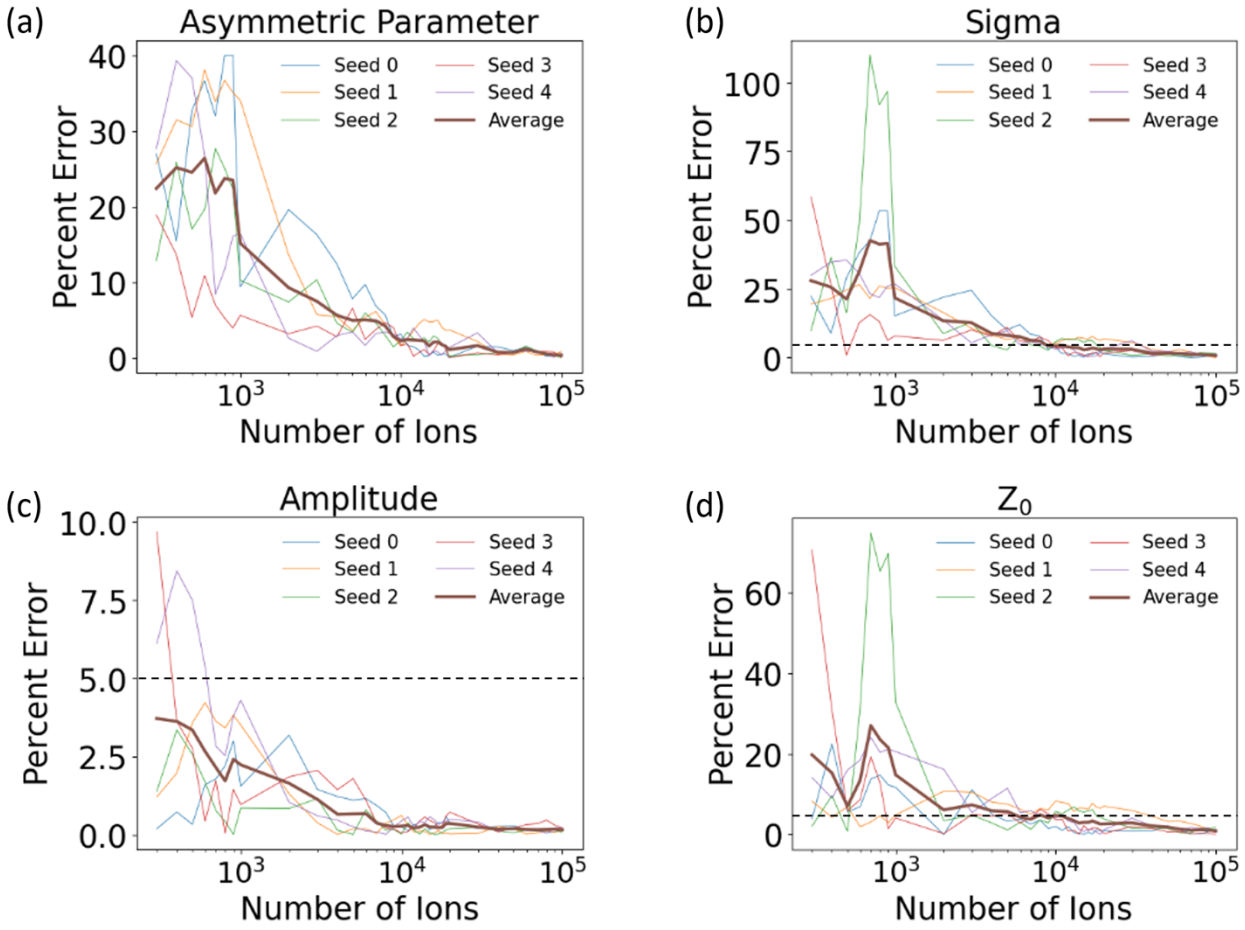

Figure 6 &

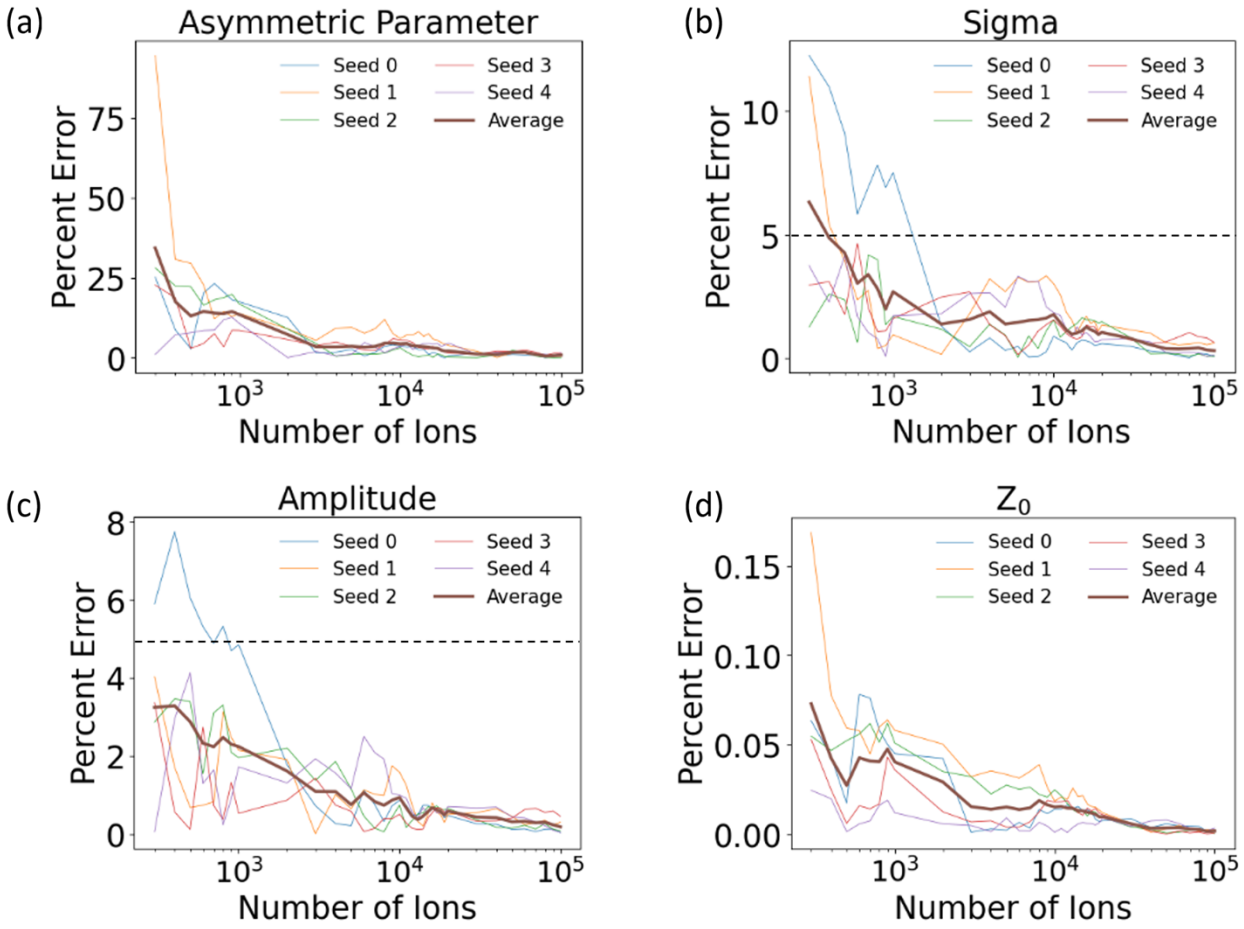

Figure 7 is the decreasing percent error of the simulation as a function of number of ions for the different fitting parameters for the vacancy data for Ga (

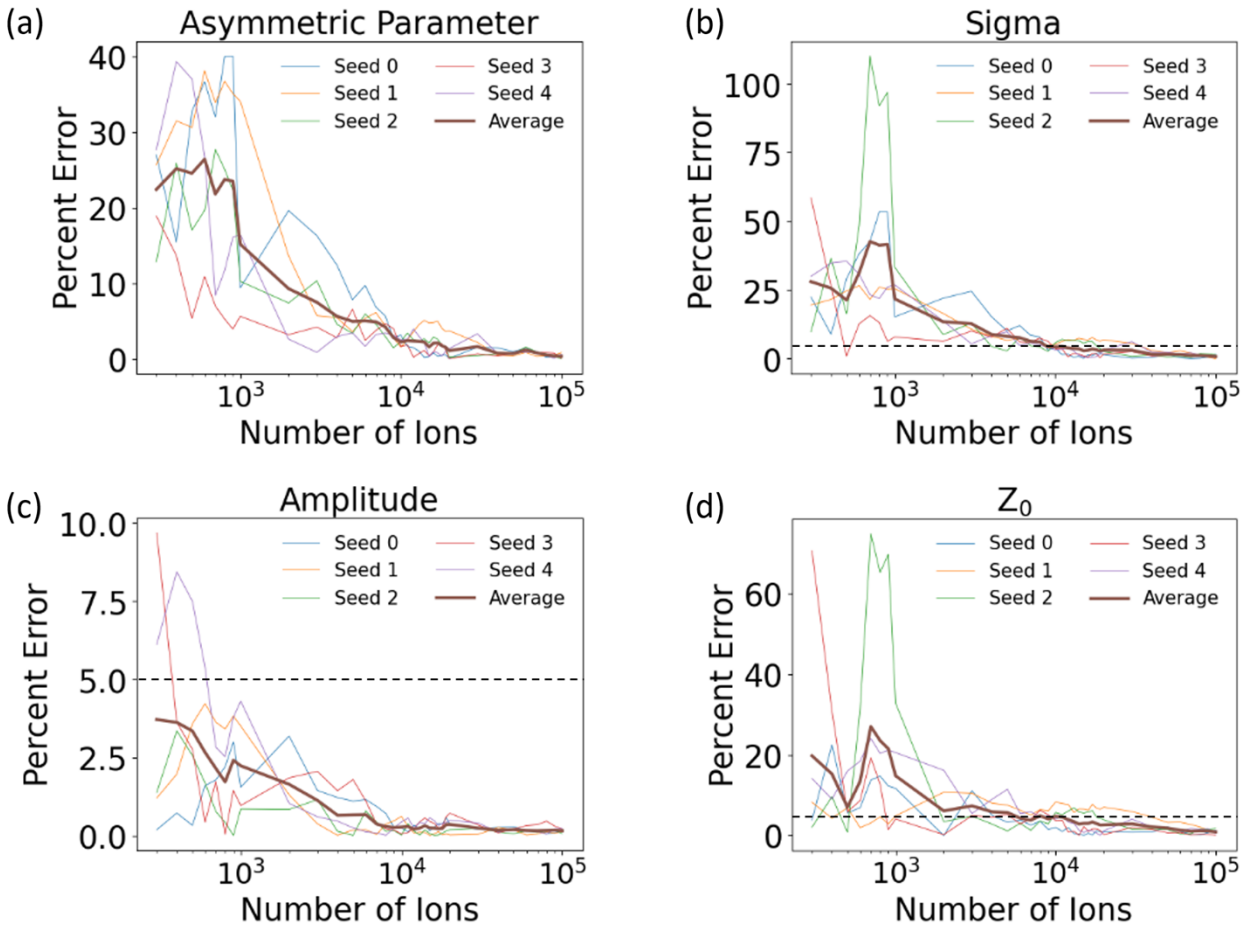

Figure 6) and C (

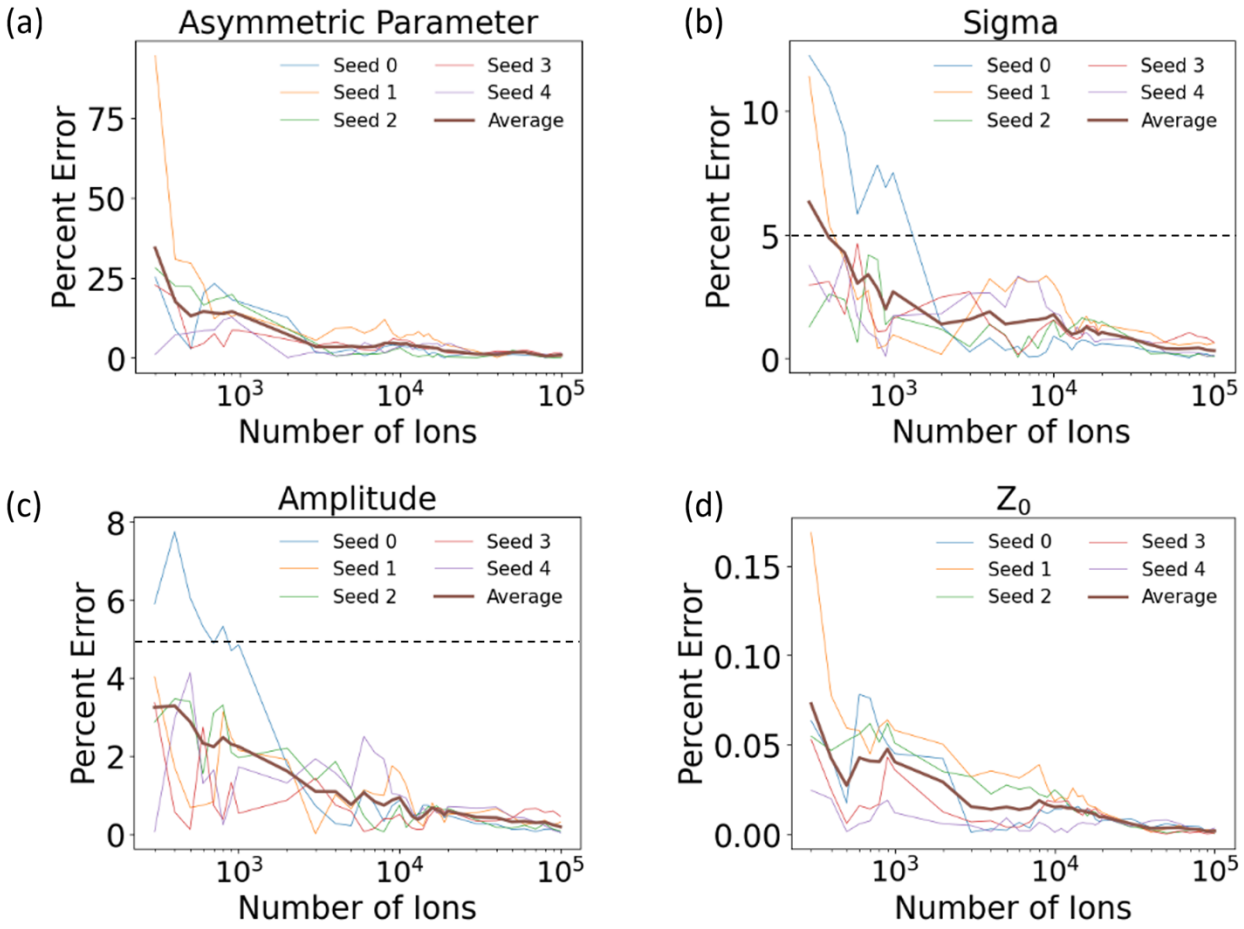

Figure 7). They show similar convergence of the fitting parameters as the number of ions increases.

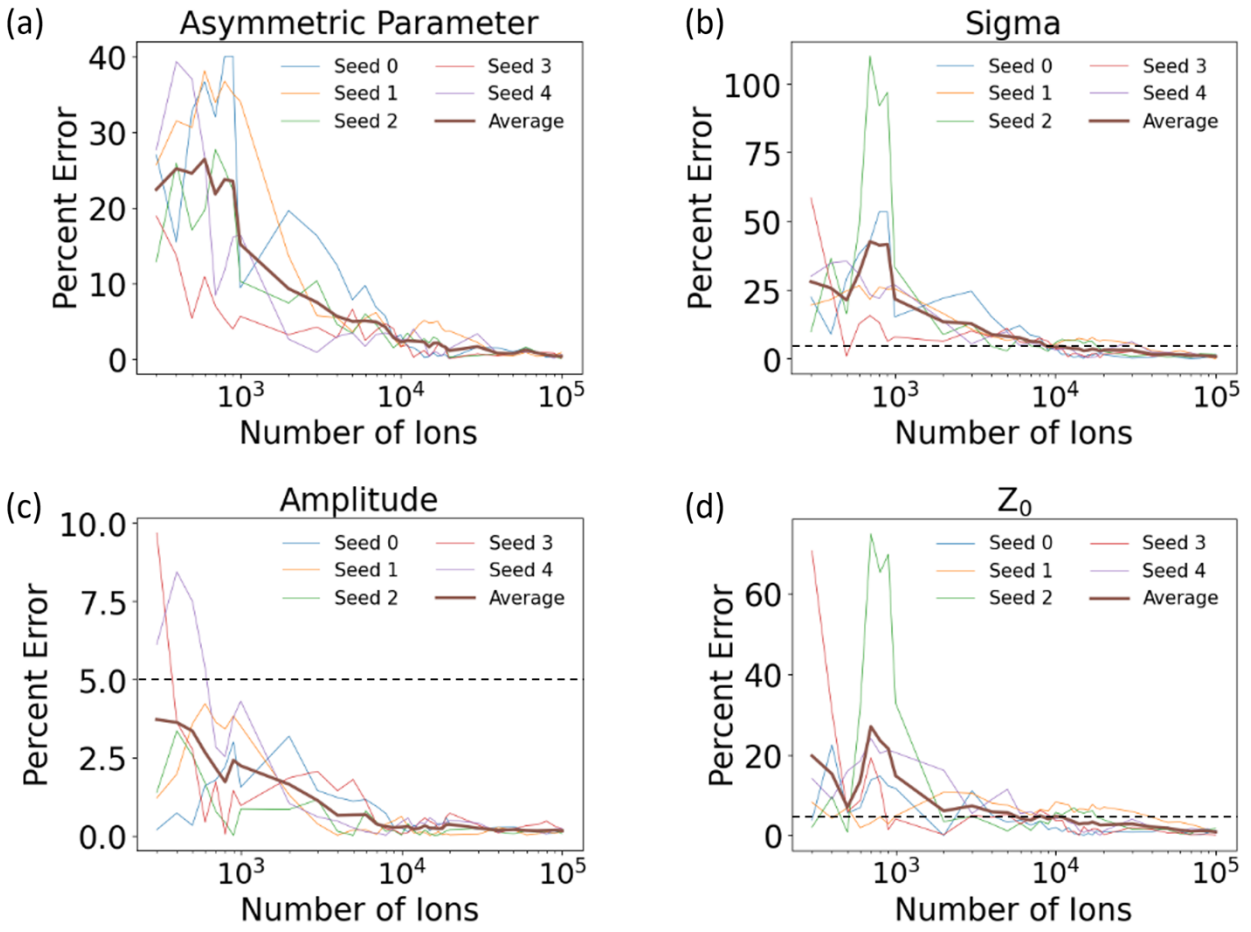

Figure 6: Percent error across an increasing number of ions the 4 fitting parameters of the asymmetric Lorentzian curve that was fit to the Ga in Si vacancy data with (a) asymmetric parameter, (b) sigma, (c) amplitude, and (d) Zo. Five different simulated seed numbers are plotted along with the average of those 5 seed numbers. The average goes towards zero faster than the individual curves indicating a better convergence when averaging multiple seeds compared to using a single seed. The dashed horizontal line denotes the 5 % error threshold. At high energy estimation of the ion range has high relative accuracy, hence all cases have a < 5 % error.

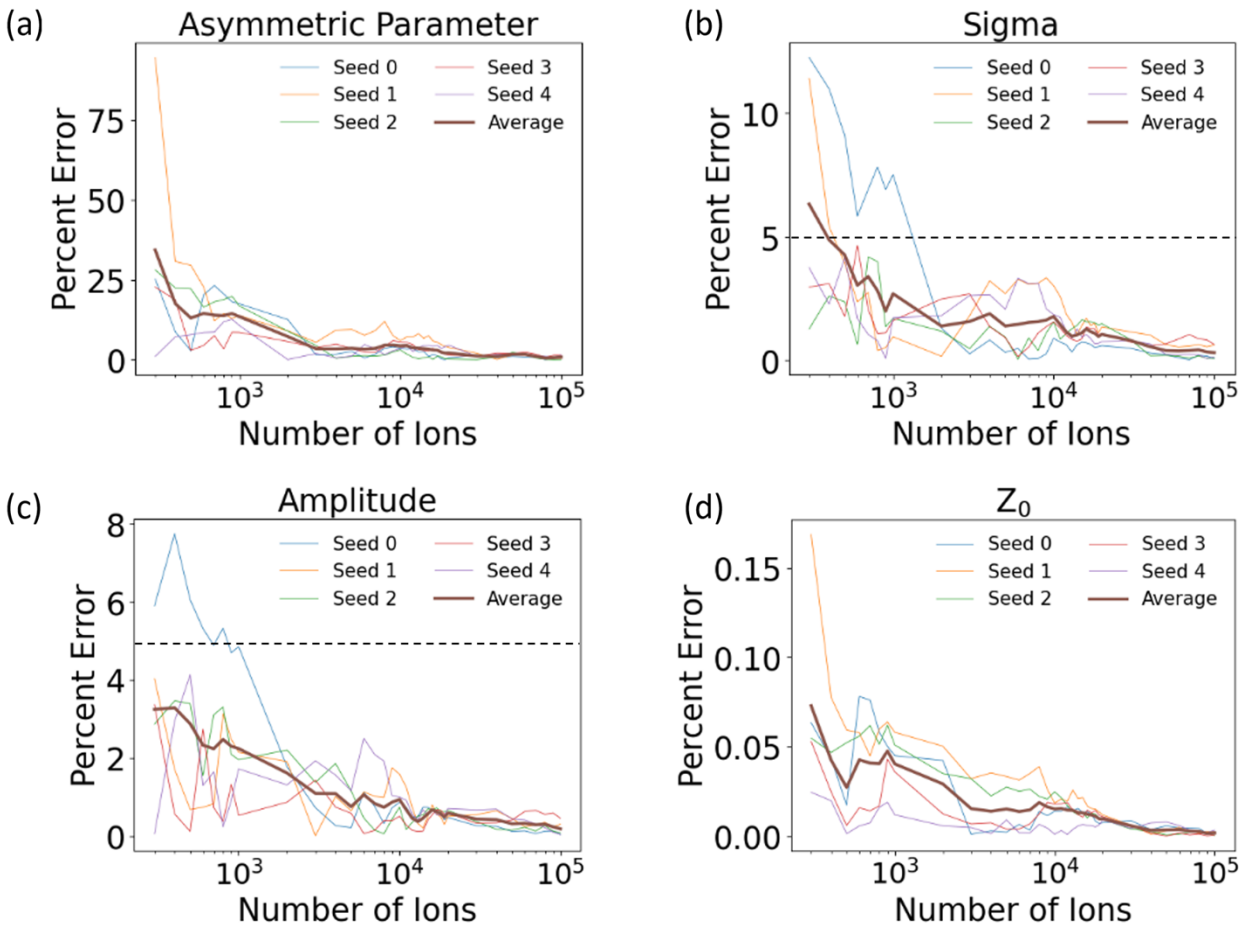

Figure 7: Percent error across an increasing number of ions the 4 fitting parameters of the asymmetric Lorentzian curve that was fit to the C in Si vacancy data with (a) asymmetric parameter, (b) sigma, (c) amplitude, and (d) Zo. Five different simulated seed numbers are plotted along with the average of those 5 seed numbers. The average goes towards zero faster than the individual curves indicating a better convergence when averaging multiple seeds compared to using a single seed. The dashed horizontal line denotes the 5 % error threshold. At high energy estimation of the ion range has high relative accuracy, hence all cases have a < 5 % error.

Since we observed an improved convergence of error for the average of all seed simulations compared to individual seeds in Figures 4-7, we examined the effect of averaging a larger number of seed simulation outputs with each seed simulating a smaller number of ions while maintaining the total number of ions simulated constant at 1e4 ions. For example, how does convergence change when averaging 5 simulation seeds with 1e4/5 = 2e3 ions in each compared to 50 seeds with 1e4/50 = 2e2 in ions each? The resulting fit parameter errors versus increasing seed numbers (and lower ions per simulation) can be found in Figure 8. The figure demonstrates that although increasing the number of simulations can initially improve the convergence, for more than 10 seed numbers the convergence suffers for all relevant parameters. This effect is ascribed to reduced statistics per individual simulation, leading to decreasing accuracy per simulation which leads to a larger error in the average value.

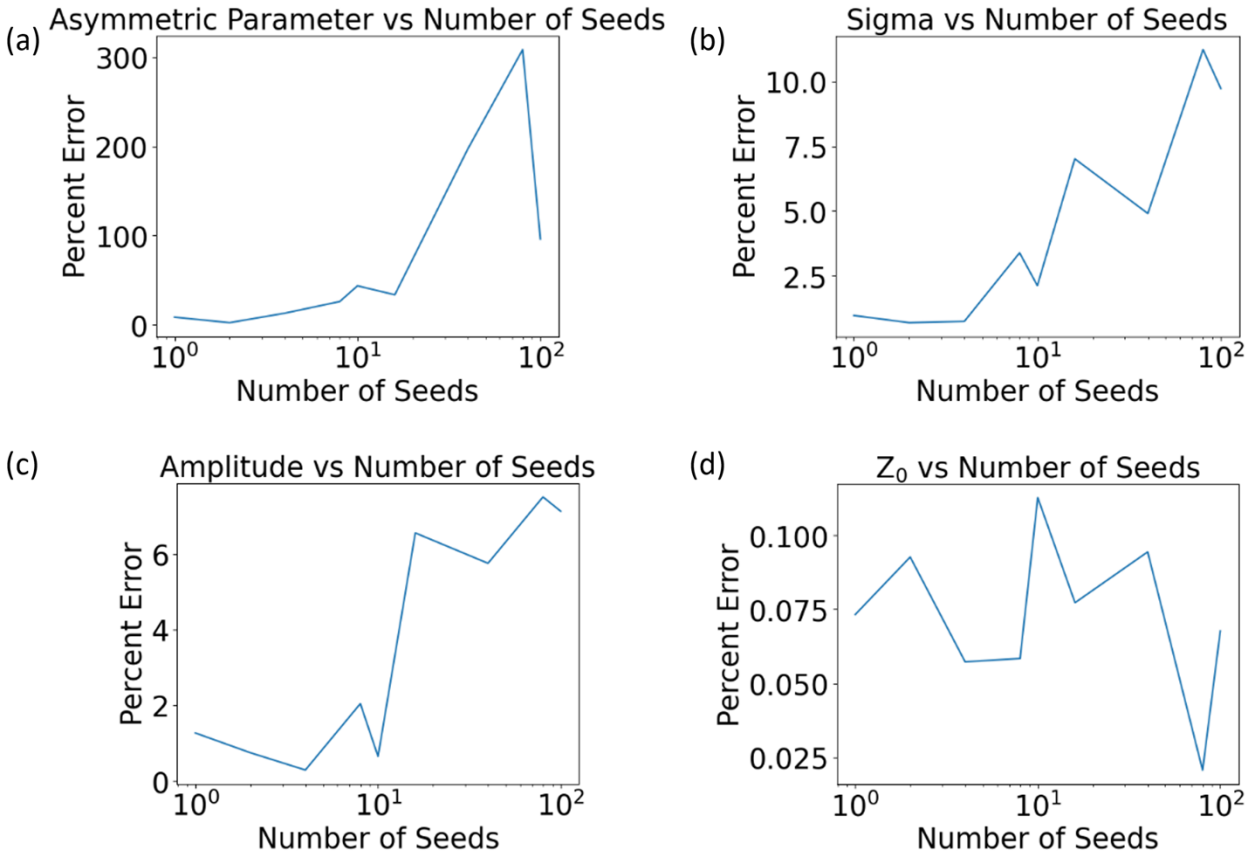

Figure 8 Error using multiple seeds while maintaining the total number of simulated ions of 1e5. (a) Asymmetric parameter, (b) Sigma, (c) Amplitude, (d) Range z0

The convergence data from the different simulations shown in Figures Figure 4-

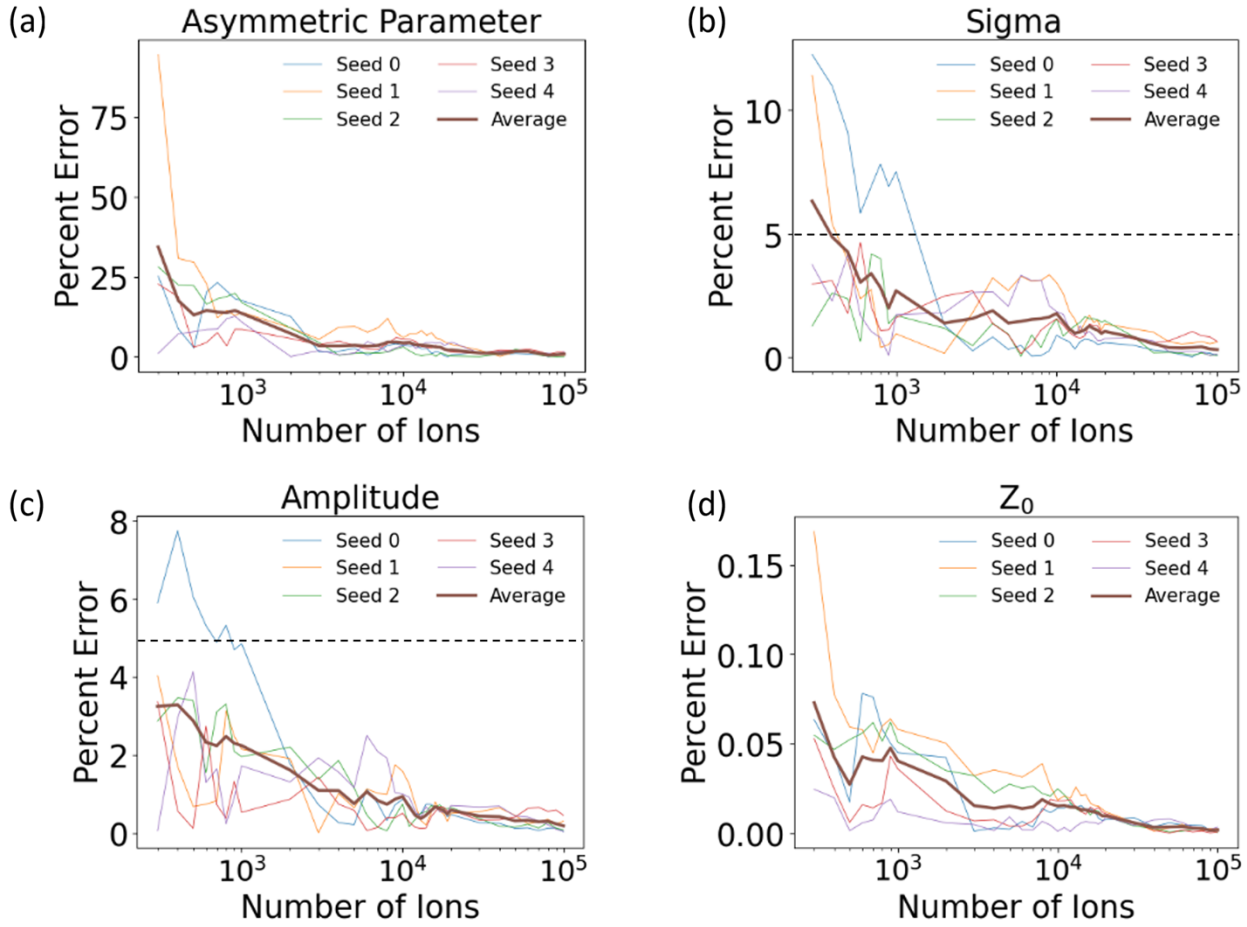

Figure 7 can be used to draw conclusions about accuracy of results versus total simulation time (number of ions) and can be used to optimize runtime for simulations. From the data in Figures 4-7, it should be noted that all 5 seeds are below 5 percent error at 10^4 ions across most fitting parameters. This indicates that for these simulation conditions, accurate results can be obtained at 10^4 ions. This decreases the runtime by a factor of 10 compared to the default SRIM setting of 10^5 ions. It was concluded that changes to the σ (sigma) parameter was the most sensitive for error reduction as a function of increase in the number of ions (aside from the asymmetric parameter) so all conclusions made on the data are based around that parameter. The large error in the asymmetric parameter can be attributed to how sensitive this parameter is in some of the simulations. The asymmetric Gaussian curve is so close to a regular Gaussian that the asymmetric parameter is very small. A small adjustment to this parameter barely changes the curve but has a large impact on the percent change of this parameter. Therefore, it is acceptable to give the asymmetric parameter a larger convergence window is some cases. By thresholding based on the sigma parameter, the low <5% percent error requirement is met in worst case scenarios for all relevant parameters.

The average of the 5 seeds is within 5 percent error at 10^3 ions across most cases, shown in Figures 4-7. Running 5 simulations of 10^3 ions gives equivalent results to running 1 simulation of 10^5 ions, when taking into account the 5% intrinsic error of SRIM. Therefore, by using the average of 5 seeds, the overall runtime can be decreased by a factor of 20 if the simulations are run back-to-back. In addition, since the single simulation is broken up into 5 independent simulations, one can also parallelize the operation,

leading to another speedup by a factor 5. In total, a factor 100 speedup can be achieved if simulations are run in parallel and only 10^3 ions are simulated per simulation.

The previous discussion regarding simulation speedup by averaging multiple simulations is summarized with examples in Table 1 and Table 2. The numbers presented in the tables represent the number of ions necessary to get to a specified percent error threshold for a single simulation compared to the average of 5 different seed simulations with lower number of simulated ions. To confidently attain the listed accuracy, it is recommended that only the listed number of ions be simulated – simulating more does not noticeably improve accuracy only increase total runtime. These tables were developed with 'worst case' assumptions so the error numbers given can be used as maximum possible error.

Table 1: Minimum number of ions required in a simulation to achieve a desired percent error for low energy simulations.

Maximum Percent Error	Single Sim (# of ions)	Average of 5 Sims with Seed 0-4 (# of ions per simulation)
5	40000	9000
10	7000	4000
20	4000	2000

Table 2: Minimum number of ions required in a simulation to achieve a desired percent error for high energy simulations.

Maximum Percent Error	Single Sim (# of ions)	Average of 5 Sims with Seed 0-4 (# of ions per simulation)
5	2000	400
10	500	<100
20	<100	<100

By examining the convergence of the simulation error, we have made key conclusions about the optimization of SRIM simulations to prioritize calculation efficiency and reduce total simulation time needed. Depending on the type of beam being simulated for either the low energy or high energy case examined in this work, we find a lower number of ions can be used to generate results with desired percent error values at 10X or 100X fewer simulated ions. Additionally, running a smaller number of ions over multiple seeds and using the mean of that data could be used to significantly decrease the runtime by parallelization.

Acknowledgements

We thank Gyorgy Vizkelethy and Edward Bielejec for internal technical review. VSV acknowledges support from the Center for Cyber Defenders at Sandia National Labs. This work was supported by the Laboratory Directed Research and Development program at Sandia National Laboratories, a multimission laboratory managed and operated by National Technology and Engineering Solutions of

Sandia LLC, a wholly owned subsidiary of Honeywell International Inc. for the U.S. Department of Energy's National Nuclear Security Administration under contract DE-NA0003525.

References

1. Williams, J.S., *Ion implantation of semiconductors.* Materials Science and Engineering: A, 1998. **253**(1): p. 8-15.
2. Orloff, J., M. Utlaut, and L. Swanson, *Applications of Focused Ion Beams*, in *High Resolution Focused Ion Beams: FIB and its Applications: The Physics of Liquid Metal Ion Sources and Ion Optics and Their Application to Focused Ion Beam Technology*. 2003, Springer US: Boston, MA. p. 205-290.
3. Hooghan, K.B.N., *Device Edits and Modifications*, in *Introduction to Focused Ion Beams: Instrumentation, Theory, Techniques and Practice*, L.A. Giannuzzi and F.A. Stevie, Editors. 2005, Springer US: Boston, MA. p. 87-106.
4. Chandrasekaran, V., et al., *High-Yield Deterministic Focused Ion Beam Implantation of Quantum Defects Enabled by In Situ Photoluminescence Feedback.* Advanced Science, 2023. **10**(18): p. 2300190.
5. Delegan, N., et al., *Deterministic nanoscale quantum spin-defect implantation and diffraction strain imaging.* Nanotechnology, 2023. **34**(38): p. 385001.
6. Wang, X., et al., *Properties of Donor Qubits in $\mathrm{Zn}\mathrm{O}$ Formed by Indium-Ion Implantation.* Physical Review Applied, 2023. **19**(5): p. 054090.
7. Lin, Y.-R., et al., *Predicting displacement damage for ion irradiation: Origin of the overestimation of vacancy production in SRIM full-cascade calculations.* Current Opinion in Solid State and Materials Science, 2023. **27**(6): p. 101120.
8. Esposito, M.G., et al., *Investigating Heavy-Ion Effects on 14-nm Process FinFETs: Displacement Damage Versus Total Ionizing Dose.* IEEE Transactions on Nuclear Science, 2021. **68**(5): p. 724-732.
9. Neuendank, J., et al. *Single Event Upset and Total Ionizing Dose Response of 12LP FinFET Digital Circuits*. in *2022 IEEE Radiation Effects Data Workshop (REDW) (in conjunction with 2022 NSREC)*. 2022.
10. Montes, J., et al., *Effect of Proton Radiation on Ultrawide Bandgap AlN Schottky Barrier Diodes.* IEEE Transactions on Nuclear Science, 2019. **66**(1): p. 91-96.
11. Ziegler, J.F. *Stopping and Range of Ions in Matter (SRIM)*. [cited 2023 02/17/2023]; Available from: srim.org.
12. Kehayias, P., et al., *Measurement and Simulation of the Magnetic Fields from a 555 Timer Integrated Circuit Using a Quantum Diamond Microscope and Finite-Element Analysis.* Physical Review Applied, 2022. **17**(1): p. 014021.
13. Kehayias, P., et al., *A fitting algorithm for optimizing ion implantation energies and fluences.* Nuclear Instruments and Methods in Physics Research Section B: Beam Interactions with Materials and Atoms, 2021. **500-501**: p. 52-56.
14. Albert Colon, B.L.D., Gyorgy Vizkelethy, Jason C. Neely, Gregory Pickrell, *Heavy Ion Single Event Burnout in High Voltage GaN P-N Diodes*, in *SAND Report*, S.N. Laboratories, Editor. 2023. p. 39.
15. Christopher Ostrouchov, Y.Z., and William J. Weber, *pysrim: Automation, Analysis, and Plotting of SRIM Calculations* Journal of Open Source Software, 2018. **3**(28).
16. Vugrin, K.W., et al., *Confidence region estimation techniques for nonlinear regression in groundwater flow: Three case studies.* Water Resources Research, 2007. **43**(3).